Synthesis, photophysical and electrochemical properties of pyridine, pyrazine and triazine-based (D–π–)$_2$A fluorescent dyes

Keiichi Imato, Toshiaki Enoki, Koji Uenaka and Yousuke Ooyama[*]

Abstract

The donor–acceptor–π-conjugated (D–π–)$_2$A fluorescent dyes **OUY-2**, **OUK-2** and **OUJ-2** with two (diphenylamino)carbazole thiophene units as D (electron-donating group)–π (π-conjugated bridge) moiety and a pyridine, pyrazine or triazine ring as electron-withdrawing group (electron-accepting group, A) have been designed and synthesized. The photophysical and electrochemical properties of the three dyes were investigated by photoabsorption and fluorescence spectroscopy, Lippert–Mataga plots, cyclic voltammetry and density functional theory calculations. The photoabsorption maximum ($\lambda_{max,abs}$) and the fluorescence maximum ($\lambda_{max,fl}$) for the intramolecular charge-transfer characteristic band of the (D–π–)$_2$A fluorescent dyes show bathochromic shifts in the order of **OUY-2** < **OUK-2** < **OUJ-2**. Moreover, the photoabsorption bands of the (D–π–)$_2$A fluorescent dyes are nearly independent of solvent polarity, while the fluorescence bands showed bathochromic shifts with increasing solvent polarity (i.e., positive fluorescence solvatochromism). The Lippert–Mataga plots for **OUY-2**, **OUK-2** and **OUJ-2** indicate that the $\Delta\mu$ (= $\mu_e - \mu_g$) value, which is the difference in the dipole moment of the dye between the excited (μ_e) and the ground (μ_g) states, increases in the order of **OUY-2** < **OUK-2** < **OUJ-2**. Therefore, the fact explains our findings that **OUJ-2** shows large bathochromic shifts of the fluorescence maxima in polar solvents, as well as the Stokes shift values of **OUJ-2** in polar solvents are much larger than those in nonpolar solvents. The cyclic voltammetry of **OUY-2**, **OUK-2** and **OUJ-2** demonstrated that there is little difference in the HOMO energy level among the three dyes, but the LUMO energy levels decrease in the order of **OUY-2** > **OUK-2** > **OUJ-2**. Consequently, this work reveals that for the (D–π–)$_2$A fluorescent dyes **OUY-2**, **OUK-2** and **OUJ-2** the bathochromic shifts of $\lambda_{max,abs}$ and $\lambda_{max,fl}$ and the lowering of the LUMO energy level are dependent on the electron-withdrawing ability of the azine ring, which increases in the order of **OUY-2** < **OUK-2** < **OUJ-2**.

Introduction

Donor–π-conjugated–acceptor (D–π–A) dyes are constructed of an electron-donating group (D) such as a diphenyl or dialkylamino group and an electron-withdrawing group (electron-accepting group, A) such as a nitro, cyano, and carboxy group or an azine ring such as pyridine, pyrazine and triazine linked by π-conjugated bridges such as oligoenes and heterocycles. Thus, the D–π–A dyes exhibit intense photoabsorption and fluorescence emission properties based on the intramolecular charge transfer (ICT) excitation from the D moiety to the A moiety [1-4]. Moreover, the D–π–A structure possesses considerable structural characteristics: the increase in the electron-donating and electron-accepting abilities of the D and A moieties and the expansion of π conjugation, respectively, can lead to a decrease in the energy gap between the HOMO and LUMO because the highest occupied molecular orbital (HOMO) is localized over the π-conjugated system containing the D moiety, and the lowest unoccupied molecular orbital (LUMO) is localized over the A moiety. Thus, the photophysical and electrochemical properties based on the ICT characteristics of D–π–A dyes should be tuneable by not only the electron-donating ability of D and the electron-accepting ability of A, but also by the elec-

tronic characteristics of the π bridge. Consequently, the D–π–A dyes are of considerable practical concern as a useful fluorescence sensor for cation, anion and neural species [5-14], an efficient emitter for organic light emitting diodes (OLEDs) [15-24], and a promising photosensitizer for dye-sensitized solar cells (DSSCs) [25-34].

Thus, in this work, to gain insight into the photophysical and electrochemical properties of D–π–A fluorescent dyes with an azine ring as electron-withdrawing group, we have designed and synthesized the (D–π–)₂A fluorescent dyes **OUY-2**, **OUK-2** and **OUJ-2** with two (diphenylamino)carbazole thiophene units as the D–π moiety and a pyridine, pyrazine or triazine ring as the A moiety (Figure 1), although we have already reported the synthesis of (D–π–)₂A fluorescent dyes **OUY-2** [2] and **OUK-2** [3,4] and their partial photopysical and electrochemical properties. One advantage of (D–π–)₂A fluorescent dyes over other D–π–A fluorescent dyes is their broad and intense photoabsorption spectral features. Herein, based on photoabsorption and fluorescence spectroscopy, Lippert–Mataga plots, cyclic voltammetry and density functional theory (DFT) calcu-
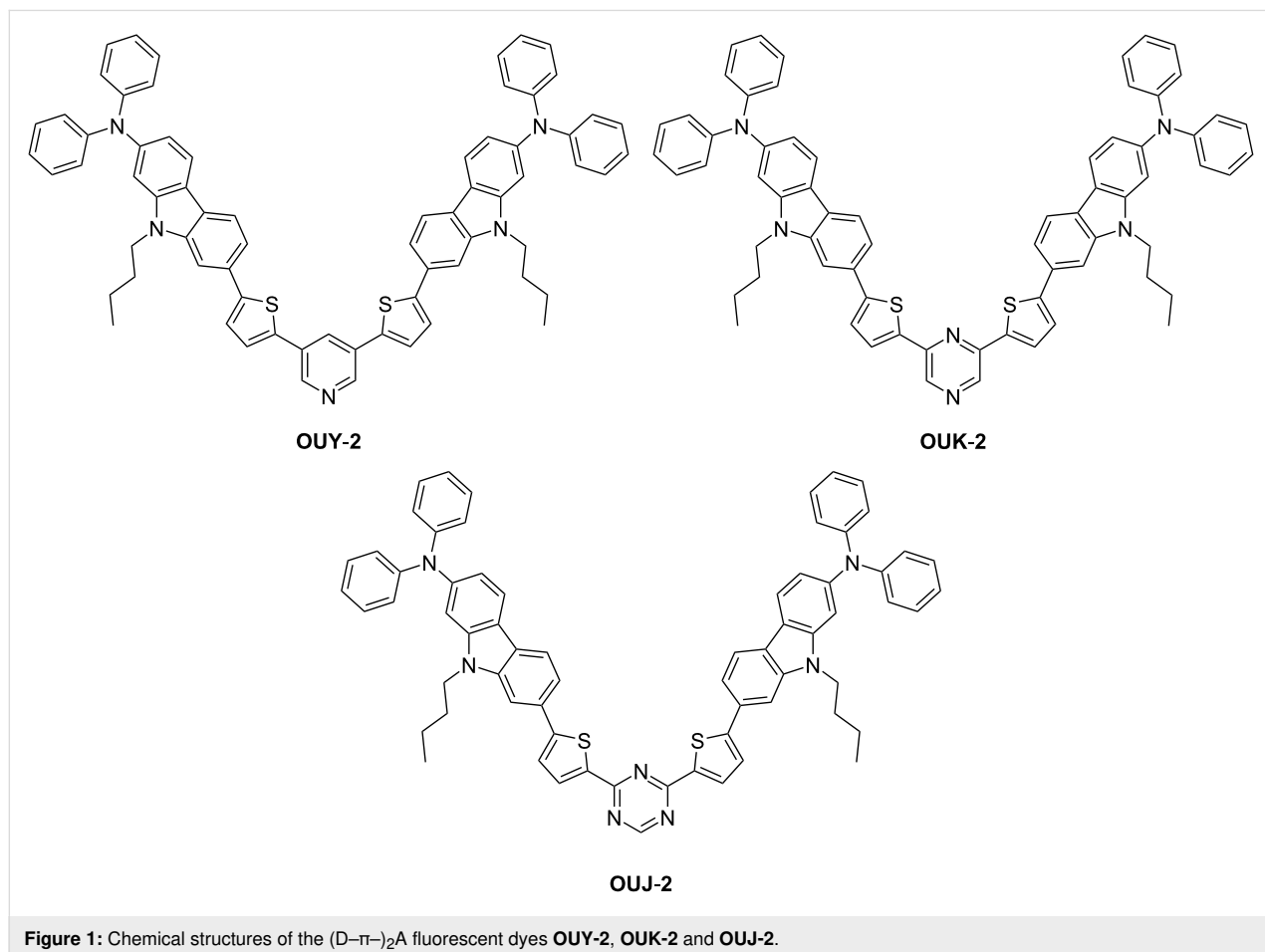

Figure 1: Chemical structures of the (D–π–)₂A fluorescent dyes **OUY-2**, **OUK-2** and **OUJ-2**.

lations, we reveal the photophysical and electrochemical properties of the (D–π–)$_2$A fluorescent dyes **OUY-2**, **OUK-2** and **OUJ-2**.

## Results and Discussion
Synthesis

The (D–π–)$_2$A fluorescent dyes **OUY-2** [2], **OUK-2** [3,4] and **OUJ-2** were prepared by Stille coupling of stannyl compound **1** [3] with 3,5-dibromopyridine, 2,6-diiodopyrazine, and 2,4-dichloro-1,3,5-triazine, respectively (Scheme 1; see Experimental section for the synthetic procedure of **OUJ-2**).

Optical properties

The photoabsorption and fluorescence spectra of **OUY-2**, **OUK-2** and **OUJ-2** in various solvents are shown in Figure 2, and their optical data are summarized in Table 1. **OUY-2**, **OUK-2** and **OUJ-2** in toluene as a non-polar solvent show the photoabsorption maximum ($\lambda_{max,abs}$) at 398 nm, 401 nm and 433 nm, respectively, which is assigned to the ICT excitation from the two (diphenylamino)carbazole thiophene units as D–π moiety to a pyridine, pyrazine or triazine ring as A moiety. For **OUK-2**, the shoulder band was observed at around 430 nm. Thus, the ICT-based photoabsorption band of the three dyes appears at a longer wavelength region in the order of **OUY-2** < **OUK-2** < **OUJ-2**, which is in agreement with the increase in the electron-withdrawing ability of the azine ring in the order of pyridyl group < pyrazyl group < triazyl group. The photoabsorption spectra of the three dyes are nearly independent of solvent polarity. This indicates that the electronic and structural characteristics of both the ground and Franck–Condon (FC) excited states do not differ much with a change in solvent polarity. The molar extinction coefficient (ε_{max}) for the ICT band is ca. 100000 M^{-1} cm^{-1} for **OUY-2**, 75000 M^{-1} cm^{-1} for **OUK-2** and 80000 M^{-1} cm^{-1} for **OUJ-2**. The corresponding fluorescence maximum ($\lambda_{max,fl}$) of the three dyes in toluene also appears at a longer wavelength region in the order of **OUY-2** (453 nm) < **OUK-2** (480 nm) < **OUJ-2** (509 nm). Interestingly, in contrast to the photoabsorption spectra, the fluorescence spectra are strongly dependent on the solvent polarity, that is, the three dyes showed a bathochromic shift of the fluorescence band with increasing solvent polarity from toluene to DMF (i.e., positive fluorescence solvatochromism). Thus, the Stokes shift (SS) values of the three dyes increase with increasing solvent polarity. Compared with **OUY-2**, **OUK-2** and **OUJ-2** exhibit significant fluorescence solvatochromic properties, that is, the two dyes show a significant decrease in the fluorescence quantum yield (Φ_f) in a polar solvent such as DMF (Φ_f = 0.59, 0.14 and 0.09 for **OUY-2**, **OUK-2** and **OUJ-2**, respectively), although in relatively low polar solvents **OUK-2** and **OUJ-2** exhibit a higher Φ_f value (0.48–0.65 and 0.72–0.86, respectively) than **OUY-2** (Φ_f = 0.38–0.58). For **OUK-2** and **OUJ-2**, the large bathochromic shifts of the fluorescence band with a significant decrease in the Φ_f value in polar solvents such as DMF might be arising from the twisted intramolecular charge transfer (TICT) excited state due to the twisting between the pyrazyl or triazyl group and the (diphenylamino)carbazole thiophene moiety, leading to non-radiative deactivation [1]. On the other hand, it is worth mentioning here
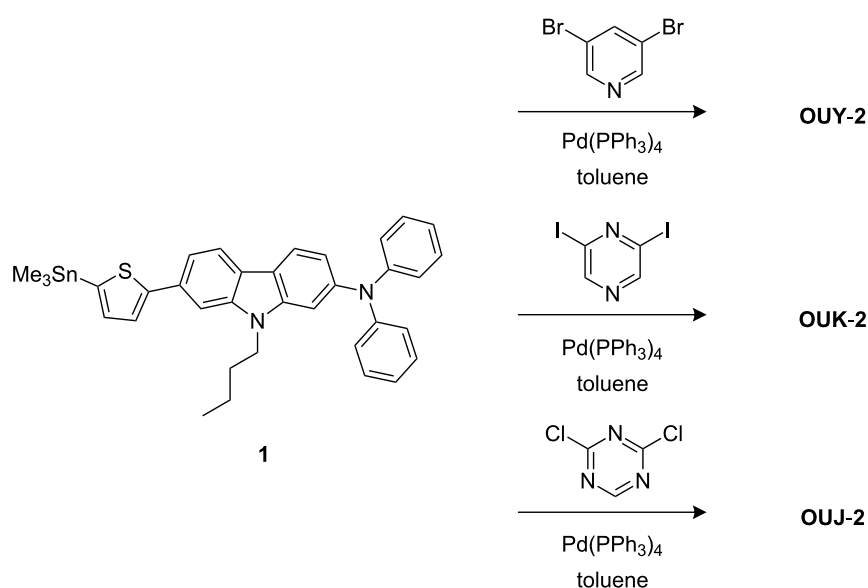
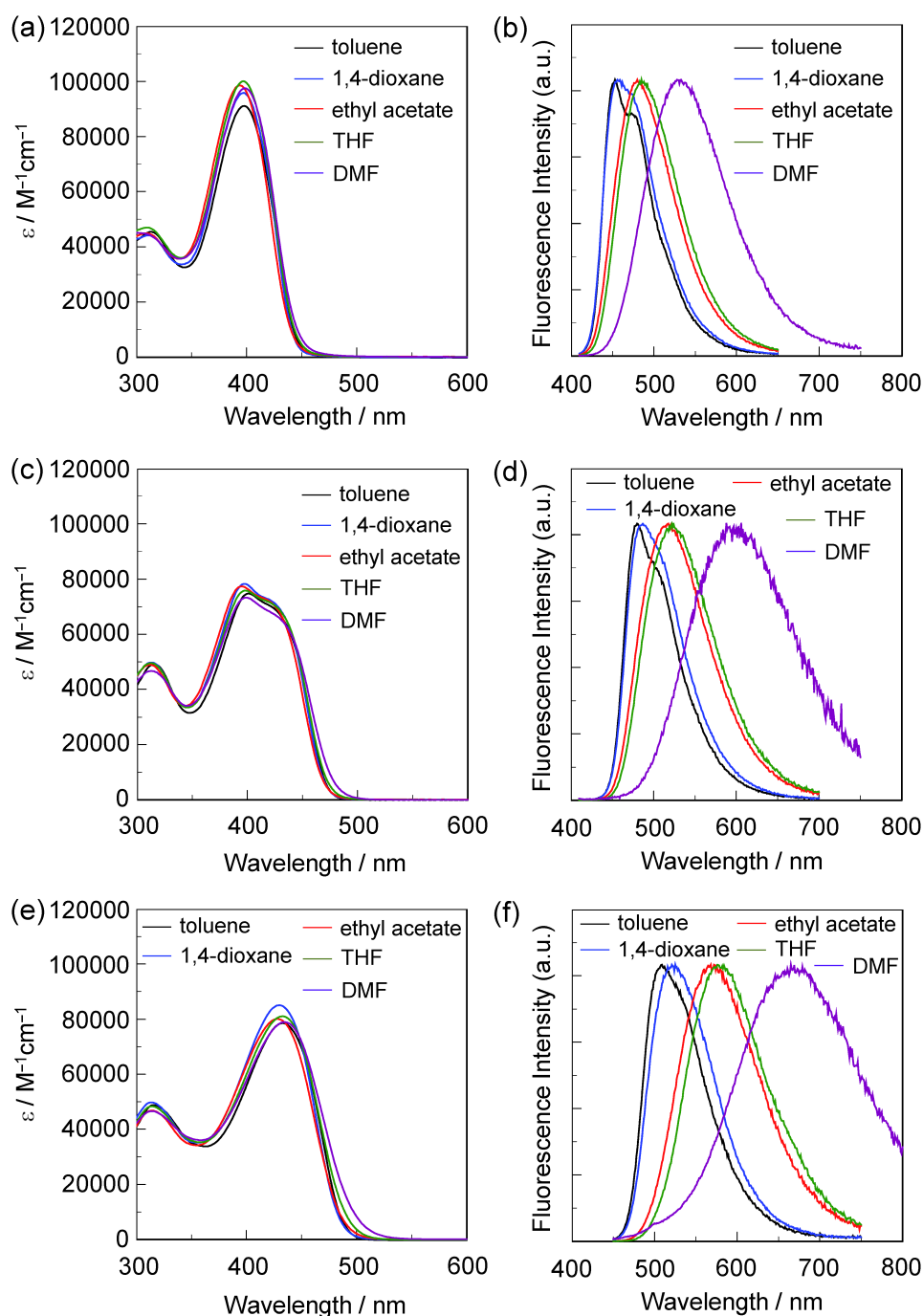**Scheme 1:** Synthesis of **OUY-2**, **OUK-2** and **OUJ-2**.

Figure 2: (a) Photoabsorption and (b) fluorescence (λ^{ex} = ca. 400 nm) spectra of **OUY-2** in various solvents. (c) Photoabsorption and (d) fluorescence (λ^{ex} = ca. 400 nm) spectra of **OUK-2** in various solvents. (e) Photoabsorption and (f) fluorescence (λ^{ex} = ca. 430 nm) spectra of **OUJ-2** in various solvents.

that the brightness values ($\varepsilon \times \Phi_f$) for **OUY-2**, **OUK-2** and **OUJ-2** in various solvents are fairly large (Table 1). Thus, the fact indicates that the $(D–\pi–)_2A$ fluorescent dyes have advantageous characteristics as emitters for OLEDs and fluorescence probes for biological imaging.

It is well accepted that the dipole–dipole interactions between the fluorescent dye and the solvent molecules are responsible for the solvent-dependent shifts in the fluorescence maxima [35-43]. Therefore, in order to understand the fluorescence solvatochromisms of **OUY-2**, **OUK-2** and **OUJ-2**, we have in-

Table 1: Optical data of **OUY-2**, **OUK-2** and **OUJ-2** in various solvents.

Dye	Solvent	$\lambda_{max,abs}$ [nm] (ε [M^{-1}cm^{-1}])	$\lambda_{max,fl}$ [nm] (Φ_f)[a]	Brightness [M^{-1}cm^{-1}]	Stokes shift [cm^{-1}]
OUY-2	toluene	398 (91100)	453 (0.38)	34600	3050
	1,4-dioxane	398 (95800)	455 (0.40)	38300	3147
	ethyl acetate	394 (98500)	480 (0.39)	38400	4547
	THF	397 (100000)	485 (0.58)	58000	4570
	DMF	399 (97500)	533 (0.59)	57500	6300
OUK-2	toluene	401 (74800)	480 (0.48)	35900	4104
	1,4-dioxane	397 (78300)	487 (0.62)	48500	4655
	ethyl acetate	398 (75800)	518 (0.55)	41700	5820
	THF	394 (77400)	524 (0.65)	50300	6296
	DMF	399 (73300)	588 (0.14)	10200	8055
OUJ-2	toluene	433 (78500)	509 (0.81)	63600	3448
	1,4-dioxane	430 (85100)	525 (0.86)	73200	4208
	ethyl acetate	428 (80100)	568 (0.72)	57700	5758
	THF	433 (81100)	576 (0.72)	58400	5733
	DMF	435 (78900)	665 (0.09)	7100	7950

[a]Fluorescence quantum yields (Φ_f) were determined by using a calibrated integrating sphere system (λ^{ex} = 400 nm for **OUY-2**, 400 nm for **OUK-2**, and 430 nm for **OUJ-2**, respectively).

vestigated the relationships between the solvent polarity-dependent shift of the fluorescence maximum and the dipole moment of dye molecule on the basis of the Lippert–Mataga equation (Equation 1) [44-46]:

$$v_{st} = \frac{1}{4\pi\varepsilon_0} \cdot \frac{2\Delta\mu^2}{hca^3} \Delta f + const.$$ (1)

where

$$\Delta f = \frac{\varepsilon - 1}{2\varepsilon + 1} - \frac{n^2 - 1}{2n^2 + 1}$$ (2)

Consequently, on the basis of Equation (1) and Equation (2), the change in the dipole moment, $\Delta\mu = \mu_e - \mu_g$, between the ground ($\mu_g$) and the excited ($\mu_e$) states can easily be evaluated from the slope of a plot of v_{st} against Δf (the Lippert–Mataga plot), where v_{st} is the Stokes shift (Table 1), ε_0 is the vacuum permittivity, h is Planck's constant, c is the velocity of light, a is the Onsager radius of the dye molecule (7.81 Å, 7.99 Å and 7.91 Å for **OUY-2**, **OUK-2** and **OUJ-2**, respectively, estimated from DFT calculation at the B3LYP/6-31G(d,p) level of theory [47]), Δf is the orientation polarizability, ε is the static dielectric constant, and n is the refractive index of the solvent. The Lippert–Mataga plots (Figure 3) for the three dyes show high linearity, indicating that for the three dyes the solvent-dependent shift in the fluorescence maximum is mainly attributed to the dipole–dipole interactions between the dye molecule and the solvent molecule. The slopes (m_{sl}) became steep in the order of

OUY-2 (10500 cm^{-1}) < **OUK-2** (12200 cm^{-1}) < **OUJ-2** (13700 cm^{-1}). The correlation coefficient (R^2) value for the calibration curve regarding the three dyes is 0.90 for **OUY-2**, 0.88 for **OUK-2**, and 0.89 for **OUJ-2**, which indicates good linearity. The $\Delta\mu$ values increase in the order of **OUY-2** (22 D) < **OUK-2** (25 D) < **OUJ-2** (26 D), which corresponds to the increase in the electron-withdrawing ability of the azine rings (pyridyl group < pyrazyl group < triazyl group). Consequently, the Lippert–Mataga plots explains our findings that **OUJ-2** shows large bathochromic shifts in its fluorescence maximum in polar solvents, as well as the SS values for **OUJ-2** in polar solvents are much larger than those in nonpolar solvents (Table 1).

In order to investigate the solid-state photophysical properties of **OUY-2**, **OUK-2** and **OUJ-2**, we have measured the solid-state fluorescence spectra of the solids (Figure 4). The $\lambda_{max,fl}$ of the as-recrystallized dyes appears at 550 nm for **OUY-2**, 592 nm for **OUK-2**, and 557 nm for **OUJ-2**, which showed a significant bathochromic shift by 97 nm, 112 nm, and 48 nm, respectively, compared with those in toluene. The solid-state Φ_f value is below 0.02 for **OUY-2** and **OUK-2** and 0.09 for **OUJ-2**, which are much lower than those in toluene. It is well known that D–π–A fluorescent dyes show bathochromic shifts of the $\lambda_{max,fl}$ and lower Φ_f values by changing from the solution state to the solid state. This fact is attributed to the delocalization of excitons or excimers due to the formation of intermolecular π–π interactions [48-51] between the dye molecules in the solid state, although we could not prepare single crystals of **OUY-2**, **OUK-2** and **OUJ-2** for the X-ray structural analysis.
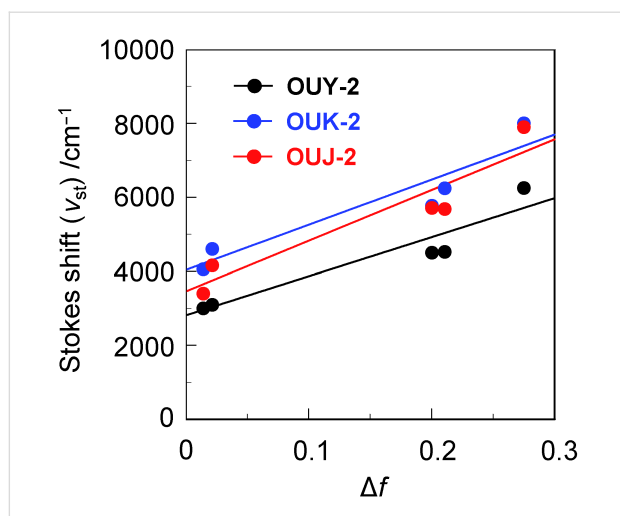
Figure 3: Correlation of the Stokes shift (ν_{st}) and the orientation polarizability (Δf) according to Equation 1 and Equation 2, respectively, for **OUY-2**, **OUK-2** and **OUJ-2**; solvent (ε, n, Δf): toluene (2.38, 1.4969, 0.0132), 1,4-dioxane (2.21, 1.4224, 0.0205), ethyl acetate (6.02, 1.3724, 0.199), THF (7.58, 1.4072, 0.2096) and DMF (36.71, 1.4305, 0.274) [4].
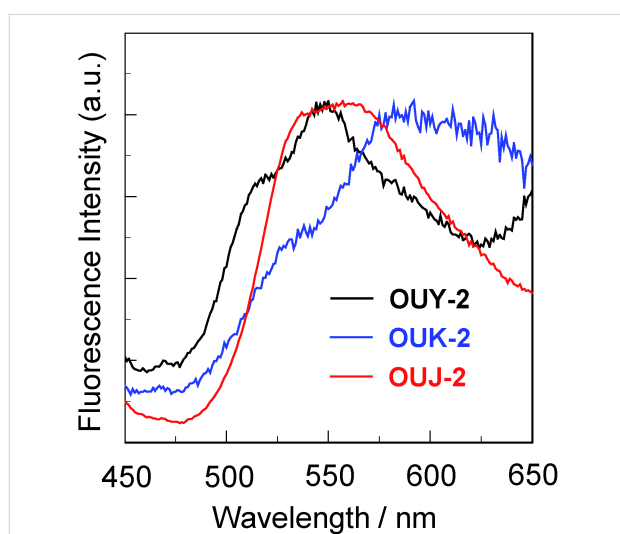

Figure 4: Fluorescence spectra of **OUY-2** (λ^{ex} = 370 nm), **OUK-2** (λ^{ex} = 370 nm) and **OUJ-2** (λ^{ex} = 380 nm) in the solid state.

Electrochemical properties

The electrochemical properties of **OUY**-2, **OUK-2** and **OUJ-2** were investigated by cyclic voltammetry (CV) in DMF containing 0.1 M tetrabutylammonium perchlorate (Bu_4NClO_4). The cyclic voltammograms of the three dyes are shown in Figure 5. The reversible oxidation waves (E_{pa}^{ox}) for the three dyes were observed at 0.42 V for **OUY**-2 and **OUK-2** and 0.45 V for **OUJ-2**, vs ferrocene/ferrocenium (Fc/Fc$^+$) (Table 2). The corresponding reduction waves (E_{pc}^{red}) appeared at 0.35 V for **OUY**-2 and **OUK-2** and 0.36 V for **OUJ-2**, thus indicating that the three dyes undergo an electrochemically stable

oxidation–reduction process. The HOMO energy level ($- [E_{1/2}^{ox} + 4.8]$ eV) versus the vacuum level was estimated from the half-wave potential for the oxidation ($E_{1/2}^{ox}$ = 0.39 V for **OUY**-2 and **OUK-2** and 0.40 V for **OUJ-2**). Therefore, the HOMO energy level was −5.19 eV for **OUY-2** and **OUK-2** and −5.20 eV for **OUJ-2**, respectively. This fact indicates that the three dyes have comparable HOMO energy levels. The LUMO energy level versus the vacuum level was evaluated from the $E_{1/2}^{ox}$ and an intersection of photoabsorption and fluorescence spectra (449 nm; 2.76 eV for **OUY-2**, 481 nm; 2.58 eV for **OUK-2**, 506 nm; 2.45 eV for **OUJ-2**) in DMF. Consequently, the LUMO energy level was obtained through equation = [HOMO + $E_{0–0}$] eV, where $E_{0–0}$ transition energy is the intersection of the photoabsorption and fluorescence spectra corresponding to the optical energy gap between the HOMO and the LUMO. Thus, the LUMO energy level versus the vacuum level lowers in the order of **OUY-2** (−2.43 eV) > **OUK-2** (−2.61 eV) > **OUJ-2** (−2.75 eV). This result demonstrates that an increase of the electron-withdrawing ability of the azine ring lowers the LUMO energy level of the (D–π–)$_2$A fluorescent dyes. Consequently, the fact revealed that the bathochromic shift of the ICT-based photoabsorption band in the order of **OUY-2** < **OUK-2** < **OUJ-2** is attributed to the stabilization of the LUMO energy level due to the increase in the electron-withdrawing ability of the azine ring in the order of pyridyl < pyrazyl < triazyl, resulting in a decrease in the energy gap between the HOMO and the LUMO.
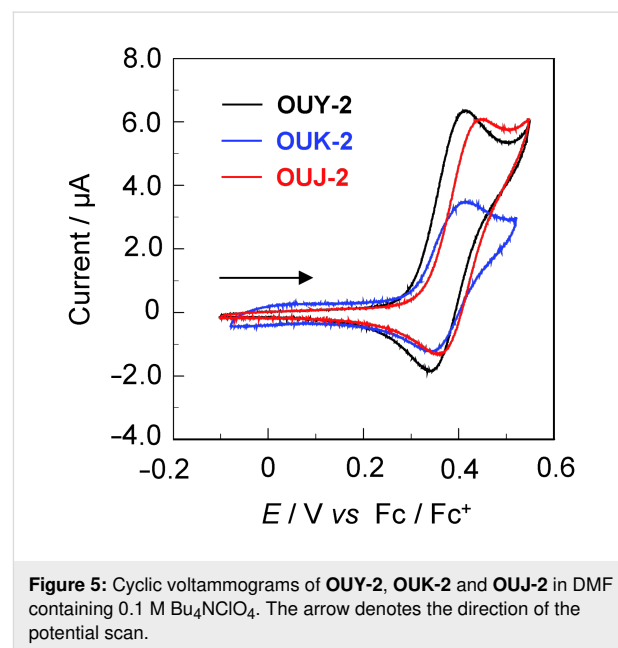

Figure 5: Cyclic voltammograms of **OUY-2**, **OUK-2** and **OUJ-2** in DMF containing 0.1 M Bu_4NClO_4. The arrow denotes the direction of the potential scan.

Theoretical calculations

In order to examine the HOMO and LUMO distributions of **OUY**-2, **OUK-2** and **OUJ-2**, the molecular structures and the

Table 2: Electrochemical data and HOMO and LUMO energy level of **OUY-2, OUK-2** and **OUJ-2.**

Dye	E_{pa}^{ox} [V][a]	E_{pc}^{red} [V][a]	$E_{1/2}^{ox}$ [V][a]	HOMO [eV][b]	LUMO [eV][c]	E_{0-0} [eV][d]
OUY-2	0.42	0.35	0.39	−5.19	−2.43	2.76 eV
OUK-2	0.42	0.35	0.39	−5.19	−2.61	2.58 eV
OUJ-2	0.45	0.36	0.40	−5.20	−2.75	2.45 eV

[a]The anodic peak (E_{pa}^{ox}), the cathodic peak (E_{pc}^{red}) and the half-wave ($E_{1/2}^{ox}$) potentials for oxidation vs Fc/Fc$^+$ were recorded in DMF/Bu$_4$NClO$_4$ (0.1 M) solution; [b]the HOMO energy level (−[$E^{ox}_{1/2}$ + 4.8] eV) versus the vacuum level was evaluated from the $E_{1/2}^{ox}$ for oxidation; [c]the LUMO energy level versus the vacuum level was evaluated from the HOMO and the optical energy gap (E_{0-0}), that is, the LUMO energy level was obtained through equation = [HOMO + E_{0-0}] eV; [d]the optical energy gap (E_{0-0}) was determined from the intersection of the photoabsorption and fluorescence spectra in DMF.

molecular orbitals of the three dyes were calculated using the DFT at the B3LYP/6-31G(d,p) level of theory [47]. The results of the DFT calculation for the three dyes indicated that the HOMO is mostly localized on the two (diphenylamino)carbazole moieties containing the thiophene ring and the LUMO is mostly localized on the thienylpyridine moiety for **OUY-2**, the thienylpyrazine moiety for **OUK-2** and the thienyltriazine moiety for **OUJ-2** (Figure 6). Accordingly, the DFT calculations reveal that the photoexcitation of **OUY-2**, **OUK-2** and **OUJ-2** induces the ICT from the two (diphenylamino)carbazole moieties to each azine ring. The HOMO energy level of the three dyes is remarkably similar to each other (−4.80 eV, −4.78 eV and −4.84 eV for **OUY-2**, **OUK-2** and **OUJ-2**, respectively), and the LUMO energy level is lowered in the order of **OUY-2** (−1.56 eV) > **OUK-2** (−1.76 eV) > **OUJ-2** (−1.98 eV), which are in good agreement with the experimental results from the photoabsorption and fluorescence spectral analyses (Figure 2) and the cyclic voltammetry (Figure 5). Thus, the experimental results and the DFT calculation strongly demonstrated that the bathochromic shift of the ICT-based photoabsorption band in the order of **OUY-2** < **OUK-2** < **OUJ-2** is attributed to a stabilization of the LUMO
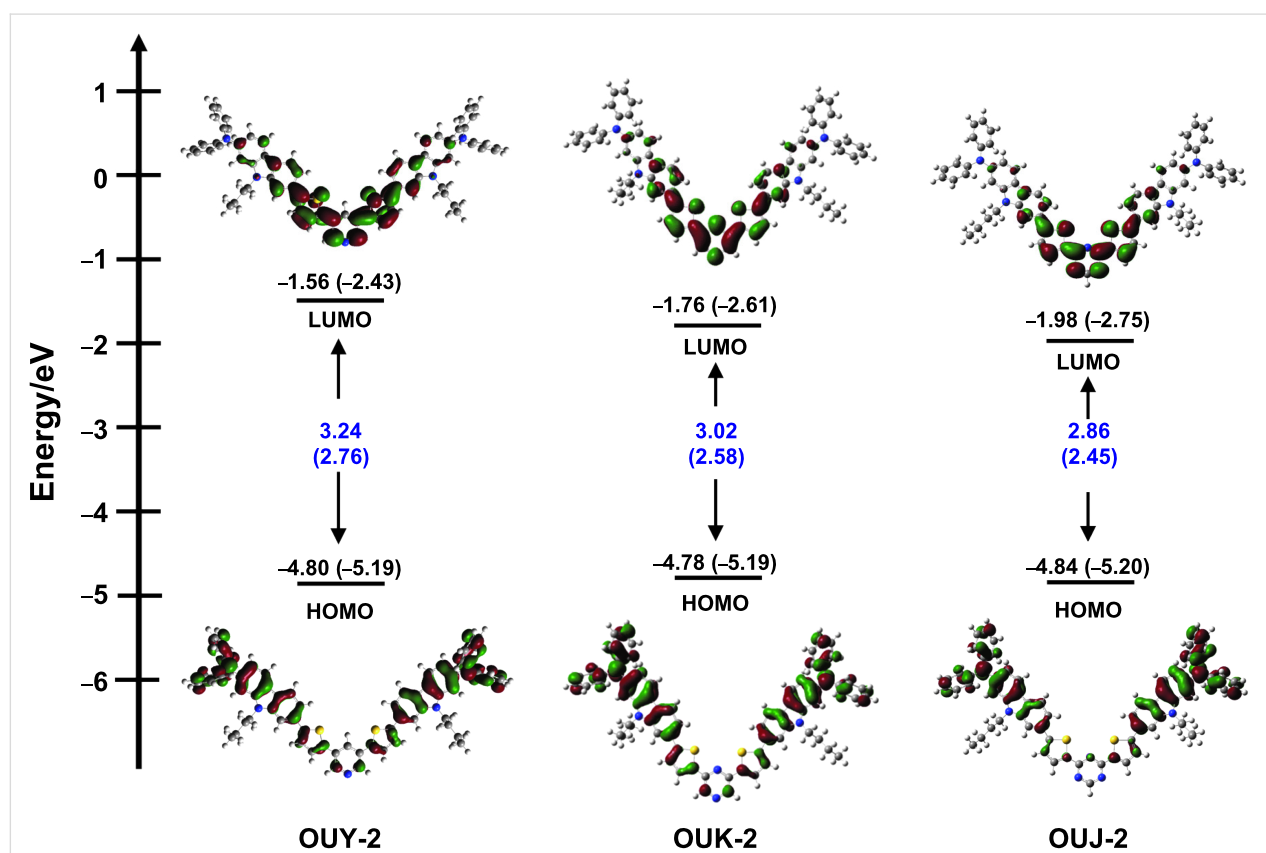

Figure 6: Energy level diagram, HOMO and LUMO of **OUY-2, OUK-2** and **OUJ-2**, derived from the DFT calculations at the B3LYP/6-31G(d,p) level of theory. Numbers in parentheses are the experimental values.

energy level due to the increase in the electron-withdrawing ability of the azine ring in the order of pyridyl < pyrazyl < triazyl.

Conclusion

To gain insight into the photophysical and electrochemical properties of D–π–A fluorescent dyes with azine rings as electron-withdrawing groups, we have designed and synthesized a new type of (D–π–)$_2$A fluorescent dyes **OUY-2**, **OUK-2** and **OUJ-2** with two (diphenylamino)carbazole thiophene units as the D (electron-donating group)–π (π-conjugated bridge) moiety and a pyridine, pyrazine or triazine ring as the electron-withdrawing group (electron-accepting group, A), and their photophysical and electrochemical properties were investigated. It was found that the intramolecular charge-transfer (ICT)-based photoabsorption and fluorescence bands of the three dyes appear at a longer wavelength region in the order of **OUY-2** < **OUK-2** < **OUJ-2**. This result is due to the increase in the electron-withdrawing ability of the azine ring in the order of pyridyl < pyrazyl < triazyl. Moreover, the (D–π–)$_2$A fluorescent dyes showed a large bathochromic shift of the fluorescence maxima with increasing solvent polarity (i.e., positive fluorescence solvatochromism). The Lippert–Mataga plots revealed that the difference in the dipole moment of the dye between the excited state and the ground state increases in the order of **OUY-2** < **OUK-2** < **OUJ-2**. Thus, the fact explains our findings that **OUJ-2** shows large bathochromic shifts of fluorescence maxima in polar solvents, as well as the Stokes shift values for **OUJ-2** in polar solvents are much larger than those in nonpolar solvents. Cyclic voltammetry and DFT calculations demonstrated that the HOMO energy levels of the three dyes are remarkably similar, but the LUMO energy level is lowered in the order of **OUY-2** > **OUK-2** > **OUJ-2**, showing that increasing the electron-withdrawing ability of the azine ring lowers the LUMO energy level of the (D–π–)$_2$A fluorescent dyes. Consequently, this work reveals that for the (D–π–)$_2$A fluorescent dyes **OUY-2**, **OUK-2** and **OUJ-2**, the bathochromic shift of photoabsorption and fluorescence maxima and the lowering of the LUMO energy levels are dependent on the electron-withdrawing ability of the azine ring which increases in the order of **OUY-2** < **OUK-2** < **OUJ-2**.

Experimental
General methods

Melting points were measured with a Yanaco micro melting point apparatus MP model. FTIR spectra were recorded on a Shimadzu IRAffinity-1 spectrometer by ATR method. High-resolution mass spectra were acquired on a Thermo Fisher Scientific LTQ Orbitrap XL. ^{1}H NMR and ^{13}C NMR spectra were recorded on a Varian-400 (400 MHz) FT NMR spectrometer. Photoabsorption spectra were measured with a Hitachi

U-2910 spectrophotometer, and fluorescence spectra were measured with a Horiba FluoroMax-4 spectrofluorometer. The fluorescence quantum yields in solution were determined by a Horiba FluoroMax-4 spectrofluorometer by using a calibrated integrating sphere system. Cyclic voltammetry (CV) curves were recorded in DMF/Bu$_4$NClO$_4$ (0.1 M) solution with a three-electrode system consisting of Ag/Ag$^+$ as reference electrode, a Pt plate as working electrode, and Pt wire as counter electrode by using an electrochemical measurement system HZ-7000 (Hokuto Denko).

Synthesis
General synthetic procedure of (D–π–)$_2$A fluorescent dyes **OUY-2**, **OUK-2** and **OUJ-2**

OUY-2 [2], **OUK-2** [3] and **OUJ-2** were prepared by Stille coupling of stannyl compound **1** [3] with 3,5-dibromopyridine, 2,6-diiodopyrazine, and 2,4-dichloro-1,3,5-triazine, respectively, by using Pd(PPh$_3$)$_4$ as a catalyst in toluene at 110 °C under an argon atmosphere (Scheme 1).

Synthesis of OYJ-2: A solution of **1** [3] (0.60 g, 0.95 mmol), 2,4-dichloro-1,3,5-triazine (0.071 g, 0.48 mmol), and Pd(PPh$_3$)$_4$ (0.18 g, 0.16 mmol) in toluene (10 mL) was stirred for 48 h at 110 °C under an argon atmosphere. After concentrating under reduced pressure, the resulting residue was dissolved in dichloromethane and washed with water. The dichloromethane extract was evaporated under reduced pressure. The residue was chromatographed on silica gel (ethyl acetate/dichloromethane 1:4 as eluent) to give **OUJ-2** (0.38 g, yield 70%) as yellow solid; mp 267–269 °C; IR (ATR) v̄: 1594, 1548, 1491 cm^{-1}; ^{1}H NMR (400 MHz, CD$_2$Cl$_2$) δ 0.89 (t, *J* = 7.3 Hz, 6H), 1.29–1.35 (m, 4H), 1.75–1.83 (m, 4H), 4.22 (t, *J* = 7.1 Hz, 4H), 6.96 (dd, *J* = 1.8 and 8.4 Hz, 2H), 7.02–7.06 (m, 4H), 7.13–7.16 (m, 10H), 7.26–7.30 (m, 8H), 7.57 (d, *J* = 4.0 Hz, 2H), 7.60–7.63 (dd, *J* = 8.1 and 1.5 Hz, 2H), 7.72 (s, 2H), 7.95 (d, *J* = 8.4 Hz, 2H), 8.04 (d, *J* = 8.1 Hz, 2H), 8.27 (d, *J* = 4.0 Hz, 2H), 9.00 (s, 1H) ppm; ^{13}C NMR (100 MHz, CD$_2$Cl$_2$) δ 14.04, 20.86, 31.47, 43.10, 105.17, 106.55, 117.52, 117.92, 118.47, 120.53, 121.40, 123.08, 123.94, 124.50, 124.79, 129.58, 130.62, 133.57, 139.41, 141.56, 142.95, 147.31, 148.55, 153.55, 167.62 ppm (one aromatic carbon signal was not observed due to overlapping resonances); HRMS–ESI (*m/z*): [M + H] $^+$ calcd. for C$_{67}$H$_{56}$N$_7$S$_2$, 1022.40331; found, 1022.40344.

Supporting Information

Supporting Information File 1
^{1}H and ^{13}C NMR spectra of **OUJ-2**.
[https://www.beilstein-journals.org/bjoc/content/supplementary/1860-5397-15-167-S1.pdf]

ORCID® iDs

Yousuke Ooyama - https://orcid.org/0000-0002-0257-6930

Preprint

A non-peer-reviewed version of this article has been previously published as a preprint doi:10.3762/bxiv.2019.22.v1

References

1. Ooyama, Y.; Uenaka, K.; Ohshita, J. *RSC Adv.* **2015,** *5,* 21012–21018. doi:10.1039/c4ra16399k
2. Ooyama, Y.; Uenaka, K.; Ohshita, J. *Eur. J. Org. Chem.* **2015,** 3713–3720. doi:10.1002/ejoc.201500341
3. Ooyama, Y.; Uenaka, K.; Harima, Y.; Ohshita, J. *RSC Adv.* **2014,** *4,* 30225–30228. doi:10.1039/c4ra03999h
4. Enoki, T.; Ohshita, J.; Ooyama, Y. *Bull. Chem. Soc. Jpn.* **2018,** *91,* 1704–1709. doi:10.1246/bcsj.20180210
5. Guliyev, R.; Coskun, A.; Akkaya, E. U. *J. Am. Chem. Soc.* **2009,** *131,* 9007–9013. doi:10.1021/ja902584a
6. Woodford, C. R.; Frady, E. P.; Smith, R. S.; Morey, B.; Canzi, G.; Palida, S. F.; Araneda, R. C.; Kristan, W. B., Jr.; Kubiak, C. P.; Miller, E. W.; Tsien, R. Y. *J. Am. Chem. Soc.* **2015,** *137,* 1817–1824. doi:10.1021/ja510602z
7. Escudero, D. *Acc. Chem. Res.* **2016,** *49,* 1816–1824. doi:10.1021/acs.accounts.6b00299
8. Saha, M. L.; Yan, X.; Stang, P. J. *Acc. Chem. Res.* **2016,** *49,* 2527–2539. doi:10.1021/acs.accounts.6b00416
9. Mahendran, V.; Pasumpon, K.; Thimmarayaperumal, S.; Thilagar, P.; Shanmugam, S. *J. Org. Chem.* **2016,** *81,* 3597–3602. doi:10.1021/acs.joc.6b00267
10. Sandeep, A.; Praveen, V. K.; Kartha, K. K.; Karunakaran, V.; Ajayaghosh, A. *Chem. Sci.* **2016,** *7,* 4460–4467. doi:10.1039/c6sc00629a
11. Black, H. T.; Pelse, I.; Wolfe, R. M. W.; Reynolds, J. R. *Chem. Commun.* **2016,** *52,* 12877–12880. doi:10.1039/c6cc06443d
12. Ji, L.; Griesbeck, S.; Marder, T. B. *Chem. Sci.* **2017,** *8,* 846–863. doi:10.1039/c6sc04245g
13. Xu, Y.; Yu, S.; Chen, Q.; Chen, X.; Li, Y.; Yu, X.; Pu, L. *Chem. – Eur. J.* **2016,** *22,* 12061–12067. doi:10.1002/chem.201601540
14. Zhou, J.; Outlaw, V. K.; Townsend, C. A.; Bragg, A. E. *Chem. – Eur. J.* **2016,** *22,* 15212–15215. doi:10.1002/chem.201603284
15. Lin, S.-L.; Chan, L.-H.; Lee, R.-H.; Yen, M.-Y.; Kuo, W.-J.; Chen, C.-T.; Jeng, R.-J. *Adv. Mater. (Weinheim, Ger.)* **2008,** *20,* 3947–3952. doi:10.1002/adma.200801023
16. Park, I. S.; Komiyama, H.; Yasuda, T. *Chem. Sci.* **2017,** *8,* 953–960. doi:10.1039/c6sc03793c
17. Duan, C.; Li, J.; Han, C.; Ding, D.; Yang, H.; Wei, Y.; Xu, H. *Chem. Mater.* **2016,** *28,* 5667–5679. doi:10.1021/acs.chemmater.6b01691
18. Huang, J.-J.; Hung, Y.-H.; Ting, P.-L.; Tsai, Y.-N.; Gao, H.-J.; Chiu, T.-L.; Lee, J.-H.; Chen, C.-L.; Chou, P.-T.; Leung, M.-k. *Org. Lett.* **2016,** *18,* 672–675. doi:10.1021/acs.orglett.5b03631
19. Zhang, Q.; Li, J.; Shizu, K.; Huang, S.; Hirata, S.; Miyazaki, H.; Adachi, C. *J. Am. Chem. Soc.* **2012,** *134,* 14706–14709. doi:10.1021/ja306538w
20. Feuillastre, S.; Pauton, M.; Gao, L.; Desmarchelier, A.; Riives, A. J.; Prim, D.; Tondelier, D.; Geffroy, B.; Muller, G.; Clavier, G.; Pieters, G. *J. Am. Chem. Soc.* **2016,** *138,* 3990–3993. doi:10.1021/jacs.6b00850
21. Hirai, H.; Nakajima, K.; Nakatsuka, S.; Shiren, K.; Ni, J.; Nomura, S.; Ikuta, T.; Hatakeyama, T. *Angew. Chem., Int. Ed.* **2015,** *54,* 13581–13585. doi:10.1002/anie.201506335
22. Sasabe, H.; Hayasaka, Y.; Komatsu, R.; Nakao, K.; Kido, J. *Chem. – Eur. J.* **2017,** *23,* 114–119. doi:10.1002/chem.201604303
23. Yao, L.; Zhang, S.; Wang, R.; Li, W.; Shen, F.; Yang, B.; Ma, Y. *Angew. Chem., Int. Ed.* **2014,** *53,* 2119–2123. doi:10.1002/anie.201308486
24. Suzuki, K.; Kubo, S.; Shizu, K.; Fukushima, T.; Wakamiya, A.; Murata, Y.; Adachi, C.; Kaji, H. *Angew. Chem., Int. Ed.* **2015,** *54,* 15231–15235. doi:10.1002/anie.201508270
25. Mishra, A.; Fischer, M. K. R.; Bäuerle, P. *Angew. Chem., Int. Ed.* **2009,** *48,* 2474–2499. doi:10.1002/anie.200804709
26. Ooyama, Y.; Harima, Y. *Eur. J. Org. Chem.* **2009,** 2903–2934. doi:10.1002/ejoc.200900236
27. Li, X.; Zheng, Z.; Jiang, W.; Wu, W.; Wang, Z.; Tian, H. *Chem. Commun.* **2015,** *51,* 3590–3592. doi:10.1039/c4cc08539f
28. Kakiage, K.; Aoyama, Y.; Yano, T.; Oya, K.; Kyomen, T.; Hanaya, M. *Chem. Commun.* **2015,** *51,* 6315–6317. doi:10.1039/c5cc00464k
29. Wu, J.; Li, G.; Zhang, L.; Zhou, G.; Wang, Z.-S. *J. Mater. Chem. A* **2016,** *4,* 3342–3355. doi:10.1039/c5ta09763k
30. Gao, Y.; Li, X.; Hu, Y.; Fan, Y.; Yuan, J.; Robertson, N.; Hua, J.; Marder, S. R. *J. Mater. Chem. A* **2016,** *4,* 12865–12877. doi:10.1039/c6ta05588e
31. Yao, Z.; Zhang, M.; Li, R.; Yang, L.; Qiao, Y.; Wang, P. *Angew. Chem., Int. Ed.* **2015,** *54,* 5994–5998. doi:10.1002/anie.201501195
32. Brogdon, P.; Giordano, F.; Puneky, G. A.; Dass, A.; Zakeeruddin, S. M.; Nazeeruddin, M. K.; Grätzel, M.; Tschumper, G. S.; Delcamp, J. H. *Chem. – Eur. J.* **2016,** *22,* 694–703. doi:10.1002/chem.201503187
33. Ooyama, Y.; Inoue, S.; Nagano, T.; Kushimoto, K.; Ohshita, J.; Imae, I.; Komaguchi, K.; Harima, Y. *Angew. Chem., Int. Ed.* **2011,** *50,* 7429–7433. doi:10.1002/anie.201102552
34. Ooyama, Y.; Sato, T.; Harima, Y.; Ohshita, J. *J. Mater. Chem. A* **2014,** *2,* 3293–3296. doi:10.1039/c3ta15067d
35. Sumalekshmy, S.; Gopidas, K. R. *J. Phys. Chem. B* **2004,** *108,* 3705–3712. doi:10.1021/jp022549l
36. Sumalekshmy, S.; Gopidas, K. R. *New J. Chem.* **2005,** *29,* 325–331. doi:10.1039/b409411e
37. Sumalekshmy, S.; Gopidas, K. R. *Photochem. Photobiol. Sci.* **2005,** *4,* 539–546. doi:10.1039/b503251b
38. Dias, F. B.; Pollock, S.; Hedley, G.; Pålsson, L.-O.; Monkman, A.; Perepichka, I. I.; Perepichka, I. F.; Tavasli, M.; Bryce, M. R. *J. Phys. Chem. B* **2006,** *110,* 19329–19339. doi:10.1021/jp0643653
39. Zhao, G.-J.; Chen, R.-K.; Sun, M.-T.; Liu, J.-Y.; Li, G.-Y.; Gao, Y.-L.; Han, K.-L.; Yang, X.-C.; Sun, L. *Chem. – Eur. J.* **2008,** *14,* 6935–6947. doi:10.1002/chem.200701868
40. Aronica, C.; Venancio-Marques, A.; Chauvin, J.; Robert, V.; Lemercier, G. *Chem. – Eur. J.* **2009,** *15,* 5047–5055. doi:10.1002/chem.200802325

41. Butler, R. S.; Cohn, P.; Tenzel, P.; Abboud, K. A.; Castellano, R. K. *J. Am. Chem. Soc.* **2009,** *131,* 623–633. doi:10.1021/ja806348z

42. Ooyama, Y.; Ito, G.; Kushimoto, K.; Komaguchi, K.; Imae, I.; Harima, Y. *Org. Biomol. Chem.* **2010,** *8,* 2756–2770. doi:10.1039/c003526b

43. Enoki, T.; Matsuo, K.; Ohshita, J.; Ooyama, Y. *Phys. Chem. Chem. Phys.* **2017,** *19,* 3565–3574. doi:10.1039/c6cp08573c

44. Lippert, E. *Z. Naturforsch., A: Astrophys., Phys. Phys. Chem.* **1955,** *10,* 541–545. doi:10.1515/zna-1955-0707

45. Mataga, N.; Kaifu, Y.; Koizumi, M. *Bull. Chem. Soc. Jpn.* **1956,** *29,* 465–470. doi:10.1246/bcsj.29.465

46. Makitra, R. G. *Reichardt, C., Solvents and Solvent Effects in Organic Chemistry, Weinheim: Wiley-VCH, 2003, 630 p.;* Russian Journal of General Chemistry, Vol. 75; Springer Science and Business Media LLC, 2005; pp 664 ff. doi:10.1007/s11176-005-0294-y

47. Both the geometry optimization and energy calculation were performed by employing density functional theory (DFT), at the level of B3LYP/6-31G(d,p) on the Gaussian09 program package, Gaussian 09, *Revision A.02,* Gaussian, Inc., Wallingford, CT, 2009.

48. Langhals, H.; Potrawa, T.; Nöth, H.; Linti, G. *Angew. Chem., Int. Ed. Engl.* **1989,** *28,* 478–480. doi:10.1002/anie.198904781

49. Yeh, H.-C.; Wu, W.-C.; Wen, Y.-S.; Dai, D.-C.; Wang, J.-K.; Chen, C.-T. *J. Org. Chem.* **2004,** *69,* 6455–6462. doi:10.1021/jo049512c

50. Ooyama, Y.; Okamoto, T.; Yamaguchi, T.; Suzuki, T.; Hayashi, A.; Yoshida, K. *Chem. – Eur. J.* **2006,** *12,* 7827–7838. doi:10.1002/chem.200600094

51. Ooyama, Y.; Hagiwara, Y.; Oda, Y.; Fukuoka, H.; Ohshita, J. *RSC Adv.* **2014,** *4,* 1163–1167. doi:10.1039/c3ra45785k